Estimation of the Repeat-Pass ALOS PALSAR Interferometric Baseline Through Direct Least-Square Ellipse Fitting

Boli Xiong, *Member, IEEE*, Jing M. Chen, Gangyao Kuang, *Member, IEEE*, and Nobuhiko Kadowaki

***Abstract*—The precise estimation of the baseline is a crucial procedure in repeat-pass interferometric synthetic aperture radar (InSAR) applications. Using the ephemeris of the satellite, a polynomial regression algorithm can fit the satellite orbit at the third or higher order with a main shortcoming that the mutual constraints among the three dimensions defining the orbit are missed. In this paper, a new approach is presented to fit the satellite orbit based on the assumption that the satellite orbit is a 3-D ellipse, which retains the relations among the three dimensions. Considering the complexity of 3-D ellipse parameters estimation, the 3-D orbit is first transformed into three 2-D ellipses. Then, the parameters of these 2-D ellipses are estimated with a direct least-square ellipse fitting method (DLS-EFM). These two orbit fitting algorithms are tested with ten sets of advanced land observation satellite phased array L-band SAR data, which were acquired in north Toronto, Ontario, Canada, from September, 2008 to January, 2009. Moreover, two of them acquired with an adjacent period were chosen to form a repeat-pass InSAR, and the corresponding baseline is calculated with the proposed method as an example. The experimental results show that the error of the satellite position using DLS-EFM is at a submetric level, which is less than one-tenth of that of the polynomial regression algorithm. Consequently, the proposed method is appropriate for the baseline estimation in spaceborne InSAR applications.**

***Index Terms*—Advanced Land Observation Satellite (ALOS) phased array L-band SAR (PALSAR), ellipse fitting, ephemeris, interferometric baseline, repeat-pass synthetic aperture radar (SAR).**

I. Introduction

With the all-weather, all-time, and large-scale imaging characteristic, synthetic aperture radar (SAR) has become an important technique in global remote surveillances and measurements. Interferometric SAR (InSAR) technique combines data recorded by different sensors or the same sensor at different times to form interferograms. Then, the phase differences of the backscattered signals can be analyzed by interfering the data observed from almost identical positions of the satellite orbit. As a result, InSAR not only contains backscatter amplitude information, but also includes the interference phase information. Therefore, this technique can provide fine-resolution and high-accuracy data for global topography mapping [1]–[3], tree height retrieval [4]–[6], soil moisture inversion [7], global forestry research [8], and so on. The baseline is the distance between the sensor's positions, while the sensor is acquiring the radar echoes of the same scene during the flights. It is a foundation of SAR interferometry and needs to be established before InSAR information is derived [9], [10]. The length of the baseline is a basic parameter for forest tree height estimation [11] or topography retrieval [12] using InSAR data. According to the height and velocity of the platform, the radar wavelength, the off-nadir angle, and the bandwidth of the radar, there is an optimal baseline to generate interferograms. For advanced land observation satellite (ALOS) as an example, when it works in the polarimetry mode with an off-nadir angle 21.5°, the bandwidth is 14 MHz, and the optimum baseline is about 938 m [2], [13]. If the baseline is too short, the fringes of the interference data will be very tight and affect the accuracy of interferometric applications. If the baseline is too long, the reference data and the repeat-pass data will lose coherence, and the interferograms could not be generated [14]. For the single-pass InSAR, the distance of the two sensors is designed to be close to the optimum baseline, and it is fixed during the flight. However, for a repeat-pass InSAR, because of the disturbance of the satellite platform, it is a challenge to control the baseline and keep it stable. Hereby, the estimation of satellite positions is an important procedure in InSAR baseline estimation.

This study aims to develop a new baseline estimation method that is more accurate than the polynomial curve fitting method, which is currently widely used in InSAR applications without information from the ground control points [15]. This paper is organized as follows. Section II gives a detailed description of the test SAR data. The next section is devoted to the introduction of the two satellite orbit fitting methods. In Section IV, the precision of the two fitting methods is compared with ten sets of ALOS phased array L-band SAR (PALSAR) data. Then, the methods on how to estimate the baseline using the fitted orbits are presented in Section V. Finally, a conclusion about the proposed method is drawn in Section VI.

Manuscript received July 22, 2010; revised January 5, 2011, June 10, 2011 and October 22, 2011; accepted December 27, 2011. Date of publication March 5, 2012; date of current version August 22, 2012. This work was supported by a Grant from the National Natural Science Foundation of China under Grant 60772045.

B. Xiong and G. Kuang are with the School of Electronic Science and Engineering, National University of Defense Technology, Changsha 410073, China (e-mail: bolixiong@gmail.com; kuangyeats@hotmail.com).

J. M. Chen is with the Department of Geography and Programming in Planning, University of Toronto, Toronto, ON M5S 1A1, Canada (e-mail: jing.chen@utoronto.ca).

N. Kadowaki is with the Mitsubishi Materials Techno Corporation, Tokyo 102-8205, Japan (e-mail: nobuhiko.kadowaki@gmail.com).

Color versions of one or more of the figures in this paper are available online at http://ieeexplore.ieee.org.

Digital Object Identifier 10.1109/TGRS.2012.2184290

0196-2892/$31.00 © 2012 IEEE

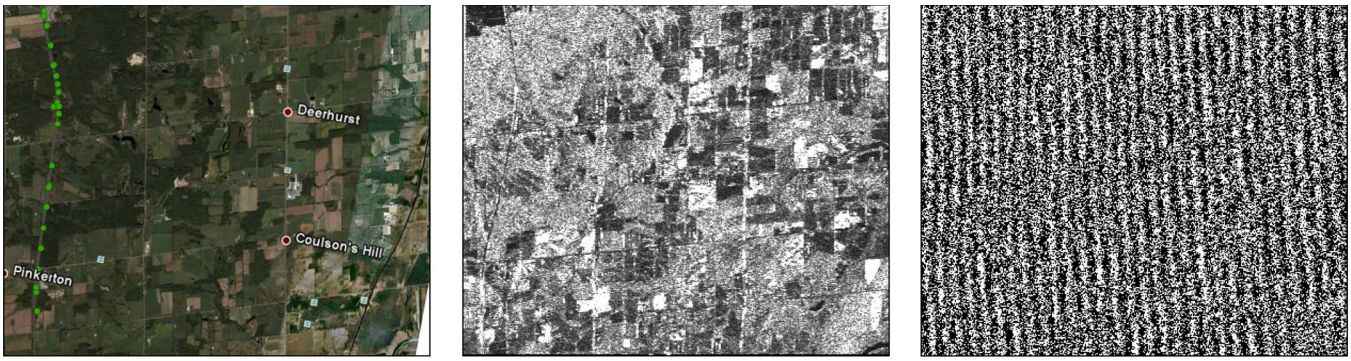

(a) (b) (c)

Fig. 1. (a) Optical image of the study area acquired from Google Earth. (b) HH polarized amplitude image acquired by ALOS PALSAR on October 8th, 2008. (c) The interferograms generated with the HH polarized complex data acquired by ALOS PALSAR on October 8th and November 23rd, 2008.

II. Data Description

The satellite ALOS was launched on January 24, 2006 by the Japan Aerospace Exploration Agency [16]. It carries a PALSAR sensor, which has the characteristics of full polarimetry, high resolution, and variable off-nadir view. The repeat-pass period of the satellite is about 46 days. It thus has the potential to use the relatively close period data as the reference and repeat-pass data to form a repeat-pass InSAR.

The study area observed by ALOS PALSAR is in north Toronto, Ontario, Canada, from September, 2008 to January, 2009. The vexcel standard single-look complex formatted data acquired in full polarimetric mode were used [13]. There are four binary data files corresponding to HH, HV, VH, and VV polarizations. Ten sets of ALOS PALSAR data were used to test the precision of the fitting methods in this paper. Two of them with an adjacent period were selected as the reference and repeat-pass data to estimate the interferometric baseline as an example. The reference data were acquired on October 8th, 2008 and the repeat-pass data were acquired 46 days later on November 23rd, 2008. Fig. 1(a) is the corresponding optical image of the study area downloaded from Google Earth (left up point: 44.2214N, 79.6702W; right down point: 44.1208N, 79.5361W). Fig. 1(b) is the HH polarized amplitude image acquired on October 8th, 2008. In order to reduce the effect of speckle noise and obtain similar nominal resolutions in the range and azimuth directions, six-look processing has been performed in the azimuth direction. After a subpixel coregistration based on the correlation coefficients, Fig. 1(c) is the corresponding interferometric image formed by calculating the coherent coefficients using a 3×3 window with the HH polarized complex data.

Each binary data file has a corresponding text header file, which records the ephemeris of the SAR sensor positions and other imaging parameters. The four header files of different polarimetric channels are almost identical. From one of them, the satellite orbit information and the imaging parameters can be obtained, which are listed in Table I as follows.

The ephemeris of ALOS contains 16 vectors of satellite position and imaging time. The position information is recorded during 15 min, almost 1 min for one record. The satellite position at a specified time could be estimated through fitting the satellite orbit using these 16 vectors. With the estimated positions of the satellite, the interferometric baseline can be calculated readily. The coordinates in each vector are recorded in Geodetic Reference System 1980 (GRS80) and will be used to fit the satellite orbit and estimate the positions of the satellite in the next section.

TABLE I
Information in the Head File (2008 October 8th)

Flight mode	Ascending	
Off Nadir angle (degree)	21.50	
Incident angle (degree)	24.00	
Pixels on range direction	1328	
Lines on azimuth direction	19227	
Center slant range	759101.95 m	
Wavelength	23.6 cm	
Time per line	0.000520000s	
The ephemeris of ALOS (totally 16 groups)	X (m)	1696514.17 m
	Y (m)	-6598423.82 m
	Z (m)	1902281.83 m
	Time (y/m/d h:m:s)	2008/10/08 03:21:00.000

III. Satellite Orbit Fitting

The estimated satellite positions directly affect the precision of the baseline estimation. In this section, a polynomial regression algorithm for fitting the satellite orbit is introduced firstly, and then the direct least-square ellipse fitting method is presented.

A. Polynomial Regression

The scheme of the baseline estimation with the polynomial regression algorithm is shown in Fig. 2.

Polynomial regression can fit a nonlinear relationship between the value of p and the corresponding value of q to describe a nonlinear phenomenon as follows:

$$q = \sum_{i=0}^{n} a_i p^i = a_0 + a_1 p + a_2 p^2 + \cdots + a_n p^n \quad n \geq 2 \quad (1)$$

where n is the polynomial regression order. The position of the SAR sensor can be seen as a function of the time, and

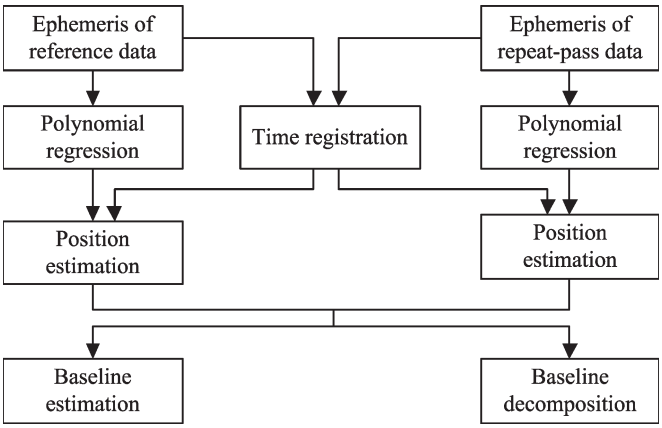

Fig. 2. Scheme of baseline estimation with the polynomial regression algorithm.

therefore the coordinates of the satellite defined by X, Y, Z can be expressed as functions of time t, and the cubic polynomial regression $(n = 3)$ between the satellite position and the time is shown in

$$\begin{cases} X = a_0 + a_1 t + a_2 t^2 + a_3 t^3 \\ Y = b_0 + b_1 t + b_2 t^2 + b_3 t^3 \\ Z = c_0 + c_1 t + c_2 t^2 + c_3 t^3. \end{cases} \tag{2}$$

B. DLS-EFM

The polynomial regression algorithm for fitting the satellite orbit only considers the relation between the coordinates and the time separately. It ignores the relations among the three dimensions. In fact, the three dimensions of a satellite orbit are related to each other, enabling the satellite to operate on an ellipse orbit around the earth. Although the earth is not a completely regular sphere, the ellipse orbit is still comparatively stable and predictable.

The scheme of the baseline estimation with an ellipse fitting algorithm is shown in Fig. 3. The differences between the schemes of the polynomial regression algorithm and DLS-EFM are the coordinate transformation and the time interpolation procedures.

Fig. 4 shows that the orbit of ALOS is a 3-D ellipse around the earth. The position of ALOS is recorded with a label in a 3-D coordinate system, while the equation of a 3-D ellipse contains ten parameters, and its expression is as follows in:

$$aX^2+bY^2+cZ^2+dXY+eXZ+fYZ+gX+hY+iZ+j=0. \tag{3}$$

When this 3-D ellipse is projected onto XOY, YOZ, and XOZ planes, three 2-D ellipses could be obtained, where each 2-D ellipse equation only contains six parameters. Therefore, it is easier to estimate the parameters of a 2-D than a 3-D ellipse. The three 2-D ellipse equations are shown in

$$\begin{cases} aX^2 + bY^2 + dXY + gX + hY + j = 0 & \text{XOY plane} \\ aX^2 + cZ^2 + eXZ + gX + iZ + j = 0, & \text{XOZ plane} \\ bY^2 + cZ^2 + fYZ + hY + iZ + j = 0, & \text{YOZ plane.} \end{cases} \tag{4}$$

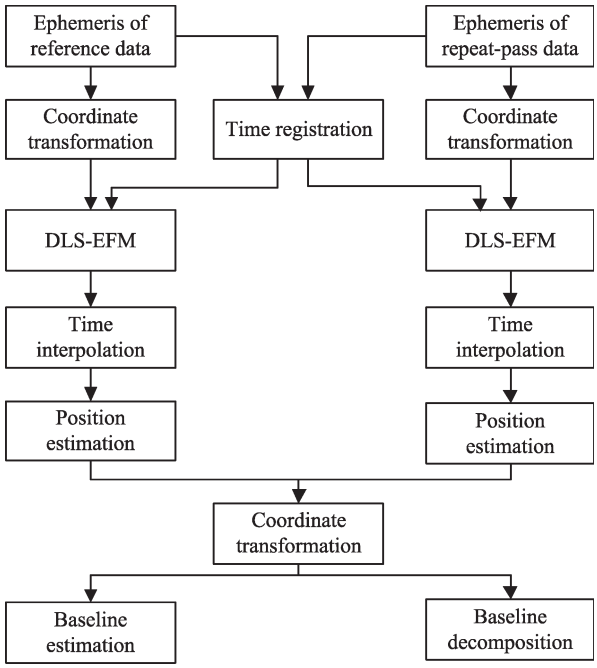

Fig. 3. Scheme of baseline estimation with DLS-EFM.

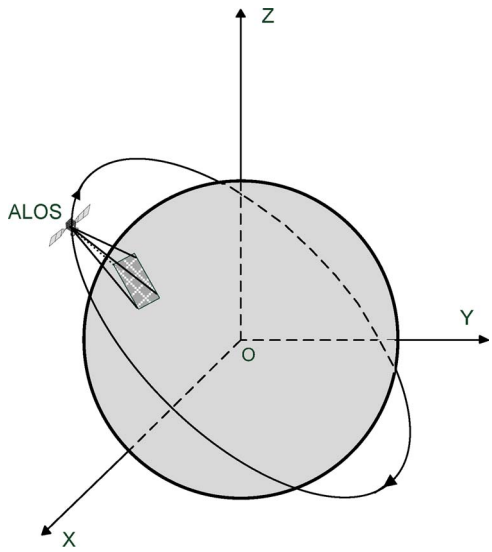

Fig. 4. Three-dimensional ellipse orbit of the ALOS around the Earth (ascending orbit).

In analytic geometry, the 2-D ellipse on the Cartesian plane is defined as a set of points (X, Y) satisfying the implicit equation in

$$AX^2 + BXY + CY^2 + DX + EY + F = 0 \times \left(F \neq 0 \& F(B^2 - 4AC) > 0 \right). \tag{5}$$

On a 2-D plane, taking XOY plane as an example, if a series of projected 2-D point labels $(X_i, Y_i),\ i = 1, 2, \ldots, K$ are acquired, the least-square error method can be used to estimate the parameters of the projected ellipse. Fitzgibbon [17] presents an algorithm named a direct least-square ellipse fitting method to estimate these six parameters of the general ellipse equation

in (5). There are mainly four steps to estimate these parameters by using K groups of position vectors of the satellite:

1) To normalize the input data $(X_i, Y_i),\ i = 1, 2, \ldots, K$;

$$mx = \frac{1}{K}\sum_{i=1}^{K} X_i \quad my = \frac{1}{K}\sum_{i=1}^{K} Y_i \tag{6}$$

$$\Delta x = \max(X_i) - \min(X_i) \quad (i = 1, 2, \cdots K) \tag{7}$$

$$\Delta y = \max(Y_i) - \min(Y_i) \quad (i = 1, 2, \cdots K) \tag{8}$$

$$\begin{cases} x_i = (X_i - mx)/\Delta x \\ y_i = (Y_i - my)/\Delta y \end{cases} \quad (i = 1, 2, \cdots K) \tag{9}$$

2) To form the column vectors, where T means matrix or vector transpose;

$$\begin{cases} \mathbf{x} = [x_1, x_2, \cdots x_K]^T \\ \mathbf{y} = [y_1, y_2, \cdots y_K]^T \\ \mathbf{xx} = [x_1 \cdot x_1, x_2 \cdot x_2, \cdots x_K \cdot x_K]^T \\ \mathbf{xy} = [x_1 \cdot y_1, x_2 \cdot y_2, \cdots x_K \cdot y_K]^T \\ \mathbf{yy} = [y_1 \cdot y_1, y_2 \cdot y_2, \cdots y_K \cdot y_K]^T \end{cases} \tag{10}$$

3) To form the scatter matrix $\mathbf{M}$ and the constraint matrix $\mathbf{R}$. $\mathbf{S}$ is a $K \times 6$ matrix and $\mathbf{M}$ and $\mathbf{R}$ are both 6×6 matrices.

$$\mathbf{S} = [\mathbf{xx}, \mathbf{xy}, \mathbf{yy}, \mathbf{x}, \mathbf{y}, \mathbf{1}] \tag{11}$$

$$\mathbf{M} = \mathbf{S}^T\mathbf{S} \tag{12}$$

$$\mathbf{R} = \begin{bmatrix} 0 & 0 & -2 & 0 & 0 & 0 \\ 0 & 1 & 0 & 0 & 0 & 0 \\ -2 & 0 & 0 & 0 & 0 & 0 \\ 0 & 0 & 0 & 0 & 0 & 0 \\ 0 & 0 & 0 & 0 & 0 & 0 \\ 0 & 0 & 0 & 0 & 0 & 0 \end{bmatrix} \tag{13}$$

4) To calculate the eigenvalues and eigenvectors with $\mathbf{S}\xi = \lambda\mathbf{R}\xi$, and then find the eigenvector ξ^* corresponding to the only negative eigenvalue λ^*, which is the estimation of the vector $\xi^* = [\tilde{A}, \tilde{B}, \tilde{C}, \tilde{D}, \tilde{E}, \tilde{F}]^T$. Therefore, the estimation of the six parameters in (5) is obtained.

IV. Comparison With the Two Fitting Methods

There are 16 groups of position vectors in each header file. Among these vectors, 15 groups are recorded at almost every integral minute, and one vector is recorded between the integral minutes. In this paper, these 15 records are used to fit the curve of the satellite orbit, and the rest record is used to evaluate the precision of the fitting algorithm as a test point.

A. Results of the Polynomial Regression Algorithm

With the 15 groups of records of the reference data, two polynomial fitting curves in X direction are shown in Fig. 5(a), where the order of the polynomial regression is eight, making $n = 8$. From Fig. 5(a), it is noted that the reference and repeat-pass curves are nearly parallel, and the distance between them could be taken as a gross estimation of the baseline. The errors

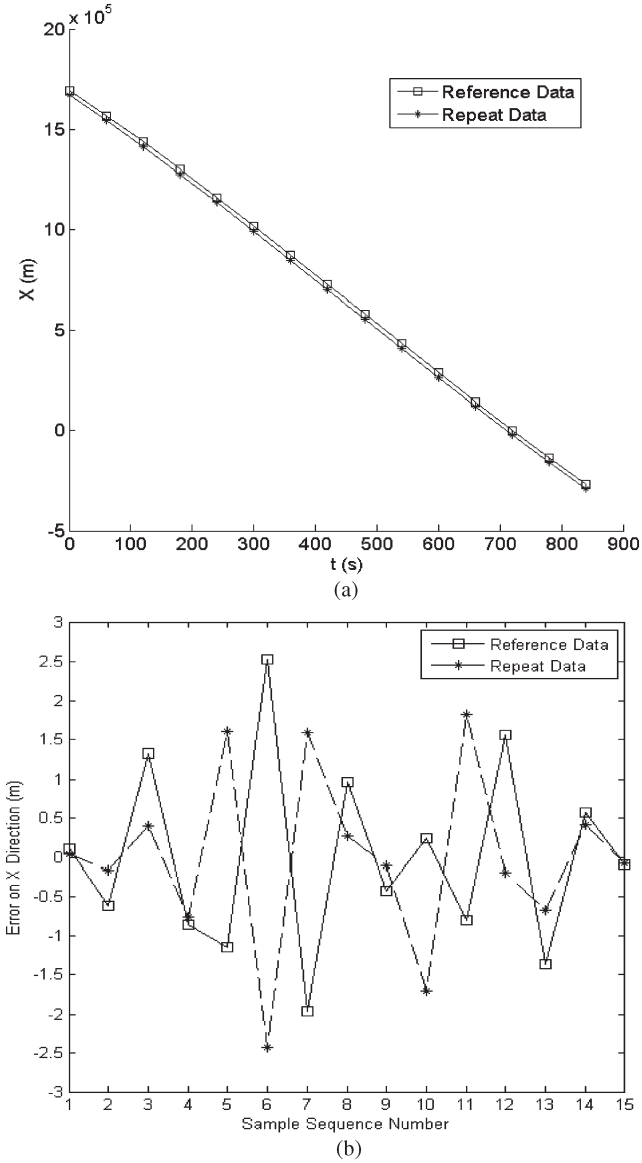

Fig. 5. (a) Polynomial fitting curves on X direction. (b) The errors of the 15 samples on X direction with polynomial regression method (both reference and repeat-pass data).

of the 15 samples on X direction with polynomial regression method are plotted in Fig. 5(b).

After getting the fitted curve parameters, the positions at the time of the test point can be estimated. The fitting error could be calculated with the distance between the observed and estimated positions of the test point. The details of estimated positions and the error of the test point with an eighth regression order are listed in Table II. The mean value and the standard derivation of the errors with the 15 samples are also listed in Table II.

B. Results of DLS-EFM

Considering that the satellite orbit is independent of the self-rotation of the earth, the coordinates of the satellite in GRS80 need to be transformed into another coordinate system, which is not influenced by the self-rotation of the earth. There is only

TABLE II
ESTIMATED POSITIONS AND ERRORS OF REFERENCE AND REPEAT-PASS DATA

Algorithm	Reference data				Repeat-pass data			
Polynomial regression (n=8)	Coordinates (m)	x	682898.93		Coordinates (m)	x	699011.61	
		y	-5217454.81			y	-5247123.04	
		z	4720534.65			z	4685163.91	
	Error of the test point	0.68292			Error of the test point	0.66837		
	Mean error of samples	3.2131			Mean error of samples	2.6308		
	Standard deviation of samples	2.1985			Standard deviation of samples	2.4743		
LSD-EFM	Coordinates (m)	XOY	x	682898.98	Coordinates (m)	XOY	x	699011.33
			y	-5217454.3			y	-5247112.25
		XOZ	x	682899.00		XOZ	x	699011.38
			z	-4720534.17			z	-4685164.22
		YOZ	y	-5217545.34		YOZ	y	-5247122.47
			z	4720534.12			z	-4685164.21
	Error of the test point	0.05426			Error of the test point	0.05449		
	Mean error of samples	0.2366			Mean error of samples	0.1897		
	Standard deviation of samples	0.1838			Standard deviation of samples	0.1212		

an angle difference between the two coordinate systems. With the new transformed coordinates and using DLS-EFM, vector ξ^* can be acquired by using the new 15 groups of transformed coordinates. Fig. 6(a) shows the ellipse on XOY plane with the reference data. The stars represent the positions of the satellite. Fig. 6(b) shows the errors of the 15 samples on X direction by using DLS-EFM with both reference and repeat-pass data.

After acquiring these six parameters of the ellipse equation, the positions of the test point can be estimated. Then, the coordinates of the test point can be transformed into GRS80 to calculate the estimation errors. The details of the estimated positions and fitting errors DLS-EFM are listed in Table II. The mean value and the standard derivation of the 15 samples are also listed in this table.

C. Comparison of the Results

From Fig. 6(a) and (b), for the reference and the repeat-pass data, the results show that the errors of the ellipse fitting algorithm are only several centimeters, whereas the errors of polynomial regressions are more than 0.5 m, i.e., 10 times greater. The optimum order for polynomial regression with a minimum error is 8. For example, the errors are 1317.97 m, 0.73 m, and 1.25 m for the orders of 3, 9, and 10 for reference data fitting, and 1340.72 m, 0.70 m, and 0.90 m for repeat-pass data fitting, respectively. The mean value and the standard derivation of the 15 samples also indicate that the proposed method is much more precise than the polynomial regression method. Another eight sets of ALOS PALSAR data are used to test the polynomial regression algorithm $(n = 8)$ and DLS-EFM. These data were all acquired in north Toronto, Ontario, Canada from September, 2008 to January, 2009 by ALOS. With different imaging parameters, the analysis of errors is listed in Table III.

From Table III, it is worth noting that that the position estimation with DLS-EFM is much more precise than that of the polynomial regression algorithm. The average error of the polynomial regression algorithm is about 8.11 m, while it is

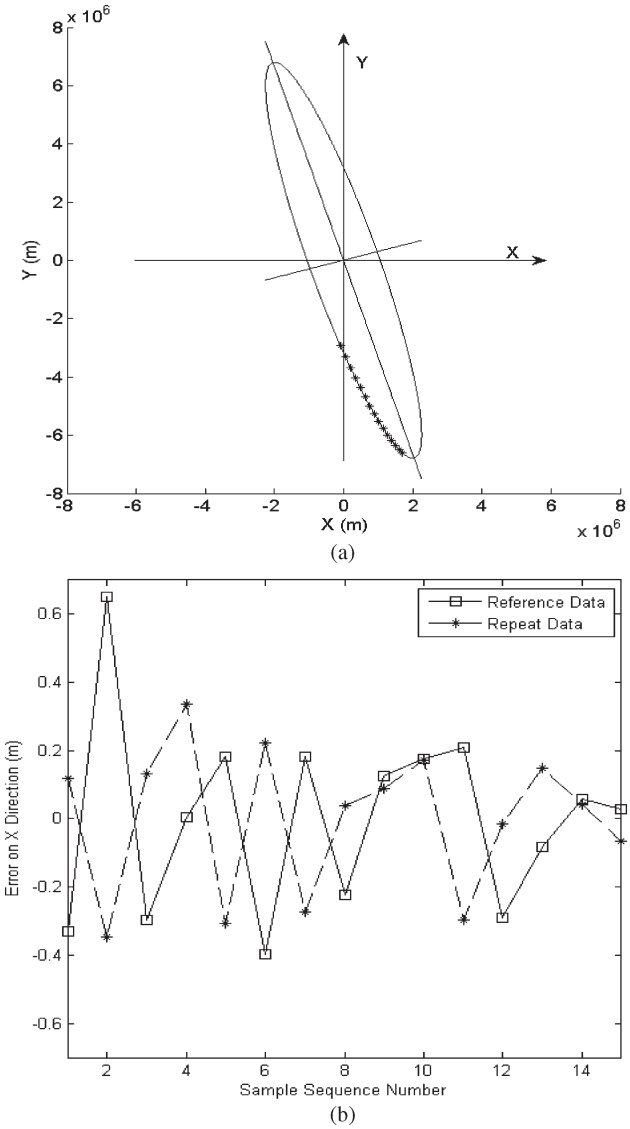

Fig. 6. (a) Ellipse fitting curve on the XOY plane with reference data acquired on October 8th, 2008. (b) The errors of the 15 samples on X direction with DLS-EFM (both reference and repeat-pass data).

TABLE III
ESTIMATED POSITIONS AND ERRORS OF DATA WITH DIFFERENT IMAGING PARAMETERS

ID	Date	Orbit number (Ascending / Descending)	Look angle	Polynomial regression			DLS-EFM		
				Error of the test point	Mean of sample errors	Standard deviation of sample errors	Error of the test point	Mean of sample errors	Standard deviation of sample errors
1	20080909	13990(A)	23.100	16.131	2.6309	2.4743	0.595	0.1691	0.1237
2	20080922	14187(D)	23.100	20.046	2.9812	2.2877	0.983	0.3955	0.2460
3	20081025	14661(A)	23.100	3.773	2.6015	2.4885	0.215	0.1857	0.1212
4	20081107	14858(D)	21.500	6.446	1.7348	2.0583	0.440	0.2724	0.1905
5	20081210	15332(A)	23.100	7.101	2.6240	2.5079	0.188	0.2107	0.1261
6	20081223	15529(D)	23.100	7.784	1.7332	2.0583	0.355	0.2658	0.1817
7	20090108	15755(A)	21.500	14.723	2.7403	2.4174	0.526	0.1686	0.1221
8	20090125	16003(A)	23.100	3.701	3.3307	2.5558	0.090	0.2184	0.1539
Average (The total 10 datasets)				8.1056	2.6221	2.3560	0.3501	0.2313	0.1582

only 0.35 m with DLS-EFM. It is obvious that the position errors of the ellipse fitting algorithm are all at a submetric level. Therefore, it is appropriate for spaceborne InSAR applications, where the baselines are generally about several hundred meters.

V. BASELINE ESTIMATION

A. Time Registration

After acquiring the parameters of the satellite orbit with the polynomial regression and ellipse fitting algorithms, time registration is the next procedure for baseline estimation. The acquiring date of reference data is 8th October, 2008, and the imaging time is 03:28:35.149392 (h:m:s), while it is 03:29:24.325631 (h:m:s) on 23rd November, 2008 for the repeat-pass data. After getting the exact imaging time, the next step is to eliminate the time difference with a precise image match. The satellite runs about 7.5 m every millisecond (ms), and the baseline of the repeat-pass spaceborne InSAR is about several hundred meters. Since one line mismatch in calibration will bring 0.52 ms time error, which approximately equals to 3.9 m of position variance, it is necessary to calibrate the imaging time precisely.

The time of acquiring the first line of the reference data and the repeat-pass data is different, which can be found in the header files. Moreover, the scenes of the first line are also different, and there is an offset by several lines. After a subpixel registration of the reference and the repeat-pass data, it was found that reference data were 0.02548s earlier than the repeat-pass data. Therefore, the time of the reference data after calibration is 03:28:35.149392 and the time of the repeat-pass data after calibration is 03:29:24.351111.

B. Baseline Estimation With Polynomial Regression

With the calibrated reference and repeat-pass time, positions of the satellite could be calculated with the curve parameters estimated using the polynomial regression algorithm. Since the time for one-scene imaging with ALOS is about 10 s, the satellite positions can be sampled every 3 s from 28:35.149392 and 29:24.351111 with the reference and repeat-pass data, respectively.

With the estimated satellite positions, the Euclidian distance formula is used to calculate the baseline B. The baseline can be projected along and across the incident direction, forming a perpendicular baseline and a parallel baseline. The perpendicular baseline $B_\perp$ is a main parameter for flat earth effect elimination in SAR interferometry [10], [18]. The relation between the number of the fringes f_n and the perpendicular baseline $B_\perp$ over a flat swath with a known width W is expressed as follows:

$$f_n = \frac{2B_\perp \cos\theta}{\lambda L} W \tag{14}$$

where θ is the off-nadir angle; λ is the wave length; and L is the slant range. With the precisely estimated baseline, the flat earth effect can be properly removed. The baseline estimation and decomposition results with the polynomial regression algorithm are listed in Table IV.

TABLE IV
POSITIONS ESTIMATED EVERY 3 s WITH POLYNOMIAL REGRESSION

	Time	Satellite position (m)		
		X	Y	Z
Reference data	28:35.149392	641417.37	-5137846.92	4812524.39
	28:38.149392	634064.85	-5123555.44	4828664.90
	28:41.149392	626712.21	-5109209.03	4844756.32
	28:44.149392	619359.53	-5094807.86	4860798.49
Repeat-pass data	29:24.351111	641797.26	-5137764.08	4812470.37
	29:27.351111	634445.34	-5123472.26	4828611.29
	29:30.351111	627093.27	-5109125.52	4844703.14
	29:33.351111	619741.16	-5094724.00	4860745.58
B	[392.56, 393.14, 393.71, 394.27]			
$B_\wedge$	[328.33, 328.76, 329.18, 329.59]			

C. Baseline Estimation With DLS-EFM

There are some differences in calculating the positions of the satellite with ellipse parameters. Time interpolation is needed before estimating satellite positions. Through a proper choice of the coordinate system, an ellipse can be described by a canonical implicit equation with the center label (0, 0), major semi-axes a, and minor semi-axes b:

$$\frac{x^2}{a^2} + \frac{y^2}{b^2} = 1. \tag{15}$$

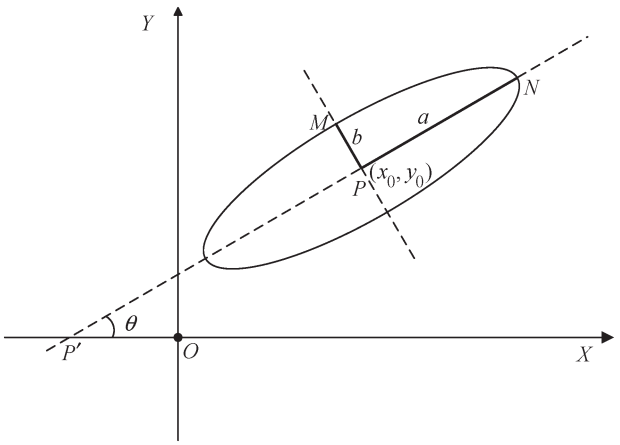

Fig. 7. Geometric parameters of a 2-D ellipse on the XOY plane.

As Fig. 7 shows, there are five geometric parameters in a 2-D ellipse equation, which are the center label (x_0, y_0), semi-major axis a, semi-minor axis b, and a rotation angle ψ. These five parameters can be deduced from the estimated vector $\xi^* = [\tilde{A}, \tilde{B}, \tilde{C}, \tilde{D}, \tilde{E}, \tilde{F}]^T$.

Make $x = a\cos\phi,\ y = b\sin\phi,\ \phi \in [0, 2\pi)$, when ϕ increases from 0 to 2π, the points (x, y) will produce a whole ellipse on the XOY plane. Therefore, for an ellipse with a rotated angle ψ and a moving center (x_0, y_0), it is simple to make the following coordinate transformation:

$$\begin{aligned} x' &= a\cos\phi\cos\psi - b\sin\phi\sin\psi + x_0 \\ y' &= a\cos\phi\sin\theta + b\sin\phi\cos\theta + y_0. \end{aligned} \tag{16}$$

When ϕ increases from 0 to 2π, these (x', y') functions plot an ellipse with the rotated angle θ, the center (x_0, y_0) and the same major and minor semi-axis a, b.

The period of the satellite around the earth is about 98.7 min, and there are 16 groups of position and imaging time information over 15 min. In order to find the exact position of the satellite at a given time, the best way is to interpolate the ellipses with the adjacent satellite positions of the given time. For example, if we need to estimate the satellite position of the reference data at 28:35.149392, the data at 27:59.999 and 29:00.000 in the reference header file could be used.

The perimeter of the satellite orbit is more than 4×10^7 m. When ϕ increases from 0 to 2π, with ϕ changing every 10^{-6} radian, the position of the satellite changes more than 6.4 m. Hence, we separate the orbit into $[2 \times \pi \times 10^9]$ segments with the step $\Delta\phi = 10^{-9}$ radian, where $[\bullet]$ means to get the nearest integer. These segments are labeled as the discrete ϕ from 0 to $[2 \times \pi \times 10^9] * \Delta\phi$. Through searching the minimum distance from the original positions to the ellipse orbit, the responding values ϕ_1, ϕ_2 can be found when they are at 27:59.999 and 29:00.000 for the reference data. The same method is used to find the discrete ϕ_3, ϕ_4 for the repeat-pass data. Then, we can use ϕ_1, ϕ_2 to estimate the value of ϕ_{ref} at 28:35.149392 for the reference data, and use ϕ_3, ϕ_4 to estimate the value of ϕ_{rep} at 29:24.351111 for the repeat-pass data. Once ϕ_{ref} and ϕ_{rep} are obtained, it is easy to define the satellite positions on the satellite orbit with those known ellipse geometric parameters.

TABLE V
POSITIONS ESTIMATED EVERY 3 s WITH DLS-EFM

	Time	Satellite position (m)		
		X	Y	Z
Reference data	28:35.149392	641417.38	-5137847.42	4812523.24
	28:38.149392	634065.25	-5123555.00	4828663.20
	28:41.149392	626712.63	-5109209.63	4844754.94
	28:44.149392	619359.96	-5094808.46	4860797.03
Repeat-pass data	29:24.351111	641797.35	-5137764.48	4812470.31
	29:27.351111	634445.45	-5123473.08	4828611.20
	29:30.351111	627093.40	-5109126.41	4844703.03
	29:33.351111	619741.30	-5094724.95	4860745.62
B	[392.09, 392.65, 393.20, 393,76]			
$B_{\wedge}$	[328.41, 328.86, 329.32, 329.77]			

Finally, these estimated satellite positions are transformed into GRS80 coordinate system and used to calculate the baseline, which are shown in Table V. From Tables IV and V, it is found that the baseline is changing during the image acquisition. Therefore, it is inappropriate to take the minimum distance between the orbits as the estimation of the interferometric baseline.

VI. CONCLUSION

In this paper, a method is developed to estimate the baseline of the spaceborne repeat-pass InSAR through transforming a 3-D satellite ellipse orbit into three 2-D ellipse curves, which employ the relations among the three dimensions. The direct least-square fitting method is adopted to estimate the parameters of these 2-D ellipses. This new satellite orbit fitting method and a conventional polynomial regression algorithm are applied to a serial of ALOS PALSAR images of an area in north Toronto, Ontario, Canada, acquired during September, 2008 and January, 2009. The experimental results show that the ellipse fitting algorithm for the satellite orbit is much better than the polynomial regression algorithm in interferometric baseline estimation. With the high-precision estimated baseline, the ALOS full polarimetric InSAR data could be used in many interferometric applications as a further study, such as DEM estimation, disaster evaluation, forest tree height inversion, and so on.

REFERENCES

[1] F. K. Li and R. M. Goldstein, "Studies of multibaseline spaceborne interferometric synthetic aperture radars," *IEEE Trans. Geosci. Remote Sens.*, vol. 28, no. 1, pp. 88–97, Jan. 1990.
[2] V. Mrstik, J. G. VanBlaricum, G. Cardillo, and M. Fennell, "Terrain height measurement accuracy of interferometric synthetic aperture radars," *IEEE Trans. Geosci. Remote Sens.*, vol. 34, no. 1, pp. 219–228, Jan. 1996.
[3] J. Baade and C. C. Schmullius, "Interferometric microrelief sensing with TerraSAR-X-first results," *IEEE Trans. Geosci. Remote Sens.*, vol. 48, no. 2, pp. 965–970, Feb. 2010.
[4] T. Mette, K. P. Papathanassiou, I. Hajnsek, and R. Zimmermann, "Forest biomass estimation using polarimetric SAR interferometry," in *Proc. Geosci. Remote Sens. Symp.*, 2002, pp. 817–819.
[5] H. Yamada, H. Okada, and Y. Yamaguchi, "Accuracy improvement of ESPRIT-based polarimetric SAR interferometry for forest height estimation," in *Proc. Geosci. Remote Sens. Symp.*, 2005, pp. 4077–4080.

[6] F. Kugler, P. P. Kostas, H. Irena, and H. Dirk, "Forest height estimation in tropical rain forest using Pol-InSAR techniques," in *Proc. Geosci. Remote Sens. Symp.*, 2006, pp. 2193–2196.
[7] M. Kurum, R. H. Lang, P. E. O'Neill, A. T. Joseph, T. J. Jackson, and M. H. Cosh, "L-band radar estimation of forest attenuation for active-passive soil moisture inversion," *IEEE Trans. Geosci. Remote Sens.*, vol. 47, no. 9, pp. 3026–3040, Sep. 2009.
[8] I. Hajnsek, F. Kugler, S.-K. Lee, and K. P. Papathanassiou, "Tropical-forest-parameter estimation by means of Pol-InSAR: The INDREX-II campaign," *IEEE Trans. Geosci. Remote Sens.*, vol. 47, no. 2, pp. 481–493, Feb. 2009.
[9] S. Suchandt, H. Runge, H. Breit, U. Steinbrecher, A. Kotenkov, and U. Balss, "Automatic extraction of traffic flows using TerraSAR-X along-track interferometry," *IEEE Trans. Geosci. Remote Sens.*, vol. 48, no. 2, pp. 807–819, Feb. 2010.
[10] R. Bamler and P. Hartl, "Topical review: Synthetic aperture radar interferometry," *Inv. Prob.*, vol. 14, no. 4, pp. 1–54, 1998.
[11] S. R. Cloude, "Robust parameter estimation using dual baseline polarimetric SAR interferometry," in *Proc. Geosci. Remote Sens. Symp.*, 2002, pp. 838–840.
[12] J. J. Mallorqui, I. Rosado, and M. Bara, "Interferometric calibration for DEM enhancing and system characterization in single pass SAR interferometry," in *Proc. Geosci. Remote Sens. Symp.*, 2001, pp. 404–406.
[13] ERSDAC, Tokyo, Japan, PALSAR Reference Guide, 2006.
[14] K. P. Papathanassiou and S. R. Cloude, "Single-baseline polarimetric SAR interferometry," *IEEE Trans. Geosci. Remote Sens.*, vol. 39, no. 11, pp. 2352–2363, Nov. 2001.
[15] H. Kimura and M. Todo, "Baseline estimation using ground points for interferometric SAR," in *Proc. IEEE Geosci. Remote Sens. Symp.*, 1997, pp. 442–444.
[16] A. Rosenqvist, M. Shimada, N. Ito, and M. Watanabe, "ALOS PALSAR: A pathfinder mission for global-scale monitoring of the environment," *IEEE Trans. Geosci. Remote Sens.*, vol. 45, no. 11, pp. 3307–3316, Nov. 2007.
[17] A. Fitzgibbon, M. Pilu, and R. B. Fisher, "Direct least square fitting of ellipses," *IEEE Trans. Pattern Anal. Mach. Intell.*, vol. 21, no. 5, pp. 476–480, May 1999.
[18] S. Peng, K. He, Y. Wang, J. Lu, J. Deng, and H. Xu, "A high accurate approach for InSAR flat earth effect removal," in *Proc. Int. Conf. Meas. Technol. Mechatron. Autom.*, Hunan, China, 2009, pp. 742–745.

Boli Xiong (S'11–M'12) received the B.S. degree in electronic engineering and the M.S. degree in photogrammetry and remote sensing from the National University of Defense Technology, Changsha, China, in 2004 and 2006, respectively, where he is currently working toward the Ph.D. degree in signal and information processing.

From 2008 to 2010, he studied at the University of Toronto, Toronto, ON, Canada as a visiting Ph.D. student. His research area is synthetic aperture radar (SAR) information processing, and his current interest is forest tree height inversion with POL-interferometric SAR and SAR image change detection.

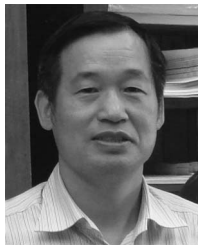

Jing M. Chen received the B.Sc. degree from the Nanjing Institute of Meteorology, Nanjing, China, in 1982 and the Ph.D. degree from Reading University, Reading, U.K., in 1986.

He is currently a Professor with the Department of Geography and Program in Planning, University of Toronto, Toronto, ON, Canada and a Senior Canada Research Chair. He has published over 180 refereed journal papers, which have been cited over 4000 times in the scientific literature. His main research interest is in remote sensing of vegetation and quantifying the role of the biosphere in the Earth system.

Dr. Chen is a Fellow of the Royal Society of Canada. He is currently an Associate Editor of the *Journal of Geophysical Research—Atmosphere*, *Canadian Journal of Remote Sensing*, and *Journal of Applied Remote Sensing*.

Gangyao Kuang (M'11) received the B.S. and M.S. degrees from the Central South University of Technology, Changsha, China, in 1998 and 1991, respectively, and the Ph.D. degree from the National University of Defense Technology, Changsha, in 1995.

He is currently a Professor and Director of the Remote Sensing Information Processing Laboratory in School of Electronic Science and Engineering, National University of Defense Technology. His current interests mainly include remote sensing, SAR image processing, change detection, synthetic aperture radar (SAR) ground moving target indication, and classification with polarimetric SAR images.

Nobuhiko Kadowaki received the M.Sc. degree in geophysics from the University of Tokyo, Tokyo, Japan, in 1995 and the Ph.D. degree in electronic engineering from the University of Electro-Communications, Tokyo, Japan, in 2007.

Since 1995, he has been an Engineer with Mitsubishi Materials Techno Corporation, Tokyo, Japan. His research interests mainly include tree height measurement using Pol-interferometric synthetic aperture radar (SAR) technique, forest classification using SAR polarimetric analysis technique, and forest biomass measurement using the microwave scattering model.